# Femtosecond wave-packet propagation in spin-orbit-coupled electronic states of $^{39,39}K_2$ and $^{39,41}K_2$

Soeren Rutz,[1] Regina de Vivie-Riedle,[2] and Elmar Schreiber[1]
[1]*Institut für Experimentalphysik, Freie Universität Berlin, Arnimallee 14, 14195 Berlin, Germany*
[2]*Institut für Physikalische und Theoretische Chemie, Freie Universität Berlin, Takustraße 3, 14195 Berlin, Germany*
(Received 22 December 1995)

Applying femtosecond pump-probe spectroscopy, we investigated via three-photon ionization (3PI) and high mass selection the vibrational dynamics of the potassium dimer's electronic $A\,^1\Sigma_u^+$ state separately for two of its isotopoes, $^{39,39}K_2$ and $^{39,41}K_2$. The fast oscillation with $T_A=500$ fs, observed for both isotopes, reflects the wave-packet propagation prepared on the potential-energy surface of the $A$ state. The long-time dynamics, however, of the isotopes is totally different. While for $^{39,39}K_2$ a beat structure with $T_{BS}=10$ ps is superimposed, for $^{39,41}K_2$ a rather fast decay and revivals at 38 ps, 60 ps, and 82 ps could be resolved. A detailed Fourier analysis of the 200-ps scans with a resolution of 0.1 $cm^{-1}$ enables the identification of the excited vibrational levels of the $A$ state in detail, including their energetic shifts due to spin-orbit coupling with the crossing $b\,^3\Pi_u$ state. Theoretical simulations of the pump-probe spectra on the basis of fully quantum-dynamical calculations reproduce well the experimental data. The reason for the slight differences can be identified as deviations between the real potential-energy surfaces and the *ab initio* data, used for the simulations and demonstrates the very high sensitivity of the femtosecond spectroscopy to investigate vibrational states and their perturbation. Furthermore, the theoretical investigations reveal the details of the ultrafast intersystem crossing process in real time. [S1050-2947(96)00607-5]

PACS number(s): 33.20.Tp, 42.50.Hz, 82.20.Tr, 36.40.−c

## I. INTRODUCTION

In recent years the dynamics of several dimers have been studied with femtosecond pump-probe techniques. These techniques opened the possibility to directly observe the vibrations and rotational revivals [1–4] of the excited molecules. The time scale for the vibrations lies in the sub-1 ps range, whereas the rotational revivals are observable after hundreds of picoseconds; e.g., in case of $I_2$ the revival of the rotation dynamics appeared after more than 600 ps [2].

Although the spectral width of ultrashort laser pulses is fairly broad, detailed spectral information could as well be deduced from the time-resolved pump-probe spectra [2,5,6]. With femtosecond multiphoton ionization spectroscopy it was possible to investigate the wave-packet dynamics in different excited states combined with different ionization pathways in $Na_2$ and $Li_2$ [4,7–9]. To simulate the ultrafast molecular dynamics in pump-probe experiments for alkali-metal-atom dimers, quantum-dynamical methods were proved to be a powerful tool [10–13]. The laser peak power dependence of the creation of wave packets on different potential-energy surfaces could be demonstrated in pump-probe experiments in $K_2$ [14]. For another alkali-metal-atom dimer, $Cs_2$, the interference of laser-induced wave packets was observable by pump, (phase) control-probe experiments [15].

From the viewpoint of classical spectroscopic experimental techniques the electronic $A\,^1\Sigma_u^+$ state of $^{39,39}K_2$ has been studied, e.g., by laser-induced fluorescence, optical-optical double resonance, and Fourier-transform spectroscopy [16–18]. Rovibrational levels could be identified and the spectroscopic constants were calculated by a Dunham fit. A Rydberg-Klein-Rees (RKR) analysis was used to deduce the potential-energy curves. A strong spin-orbit coupling between the $A\,^1\Sigma_u^+$ state and the $b\,^3\Pi_u$ state was observed around $v=12$ [16,18]. In $^{39,41}K_2$ a couple of fluorescence lines could be identified [19]. The influence of intersystem crossing (ISC) processes on the molecular dynamics has been pointed out theoretically for some examples [20–23].

Our special interest was focused on the intersection of the intersystem crossing of the $K_2$ $A\,^1\Sigma_u^+$ state with the $b\,^3\Pi_u$ state. Applying one-color pump-probe spectroscopy with a wave length of 833.7 nm, we studied the wave-packet dynamics directly around $v=12$ in $^{39,39}K_2$. The isotope-selective detection allowed us to compare the results with the heavier isotopoe $^{39,41}K_2$. With quantum-dynamical simulations we were able to simulate the results and to discuss the mechanism of the perturbation by a $^3\Pi_u$ state. We will prove that the temporal evolution of the wave-packet dynamics is strongly influenced by an ISC process.

## II. EXPERIMENT

Femtosecond laser pulses of 90 fs duration [full width at half maximum (FWHM), assuming $sech^2$ pulse shape] were generated in an argon-ion laser-pumped regeneratively titanium: sapphire laser (Spectra Physics model 2080, all lines visible, 8 W, and model 3960). The spectral width of the femtosecond pulse spectrum at the wave length 833.7 nm was measured, covering 190 $cm^{-1}$ (FWHM), so the pulses reached 1.6 times the Fourier limit (see Fig. 1). The pulse repetition rate was about 80 MHz. A Michelson-like arrangement was used to split the laser beam and to realign it collinearly with the same polarization, using single stack dielectric beam splitters. The length of one of the Michelson branches was controlled by a computer-driven dc-motor translation stage. Its position defined the delay time $\Delta t$ between pump and probe pulse and was read out by an optical encoder. The resolution of the delay time $\Delta t$ was about 0.1 fs and the minimal step width amounted to 0.3 fs. Each of the

 

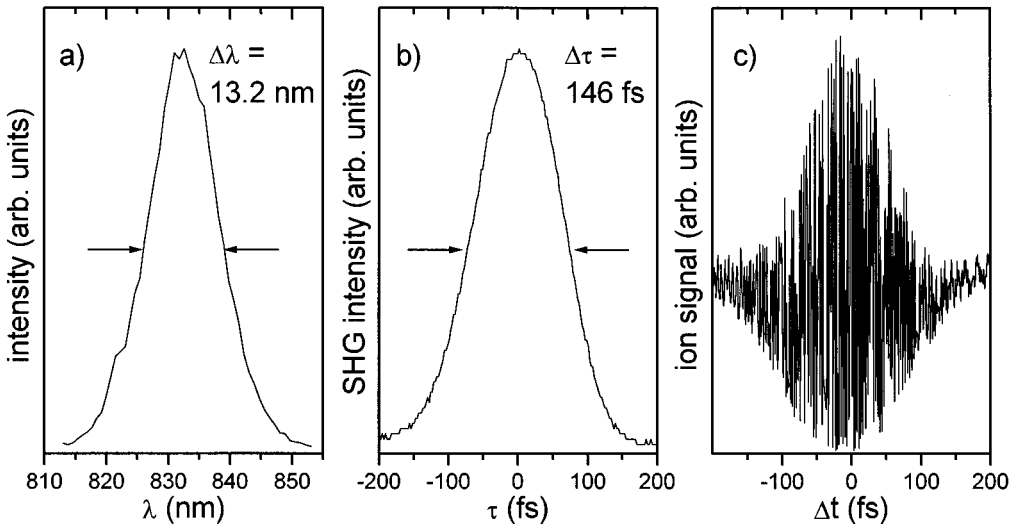


FIG. 1. Laser pulse parameters of the laser used in the experiments represented by a typical spectrum (a), and by an autocorrelation trace (b) being recorded with a second harmonic generation medium. Part (c) displays an autocorrelation trace directly recorded at the place of the laser's interaction with the molecular beam. Here, as in a common pump-probe experiment, the ion signal ($K_2^+$) is plotted as a function of the delay time.

laser pulse trains had an average power of about 200 mW.

In order to produce a molecular beam of high stability, pure potassium was evaporated at a temperature of 850 K in a TZM (titanium-zirconium-molybdenum) oven. The alkali-metal vapor was coexpanded with an inert carrier gas through a 70-$\mu$m nozzle. In this continuous supersonic beam source the rotational and vibrational temperatures amounted to about 10 and 50 K, respectively. Therefore, the $K_2$ molecules, arriving from the oven, were in the ground state $X\,^1\Sigma_g^+$. Their vibrational quantum number was $v=0$ and their rotational quantum number is $J\approx 20$.

The laser beams were focused on the molecular beam by means of a 400-mm quartz lens. Each pulse reached a peak power of about 0.5 GW cm$^{-2}$. Photoionized potassium dimers were mass-selectively detected by a quadrupole mass spectrometer with a resolution of $m/\Delta m>240$, being sufficient to distinguish between $^{39,39}K_2$ and the heavier $^{39,41}K_2$ isotopoe. The amount of each isotope ion was continuously recorded as a function of the delay time between pump and probe pulse. The result is a so-called real-time or pump-probe spectrum $I(\Delta t)$ of the three-photon ionization (3PI) process.

We chose a typical time step for the pump-probe experiments for $K_2$ of $\Delta t_{\text{step}}=50$ fs. For this step width the Nyquist critical frequency $\omega_c=1/2\Delta t_{\text{step}}c=333$ cm$^{-1}$ is even larger than four times the expected frequency $\omega_0\approx 65$ cm$^{-1}$. Therefore, an aliasing of realistic frequency components larger than $\omega_c$ is not expected in a Fourier analysis. The time to record a transient spectrum up to 200 ps was about 2 h, a time where the molecular beam is not *a priori* stable. While in our experiments the intensity of the laser was stable within 3% of the Langmuir-Taylor detector controlled intensity of the molecular beam varied over a range of about $\pm 20\%$. Therefore, we normalized the transient data to obtain data points oscillating around the zero line to perform a correct real Fourier analysis.

## III. THEORETICAL CONSIDERATIONS

In the present studies of the molecular dynamics in the $K_2$ $A\,^1\Sigma_u^+$ state, spin-orbit interaction effects become important. They enable the intersystem crossing process between the two crossing potential-energy surfaces (PES) $A\,^1\Sigma_u^+$ and $b\,^3\Pi_u$ (see Fig. 2). During the pump-probe process a wave packet is prepared in the $A$ state. According to the electronic state selection rules, the $b$ state is dark during femtosecond

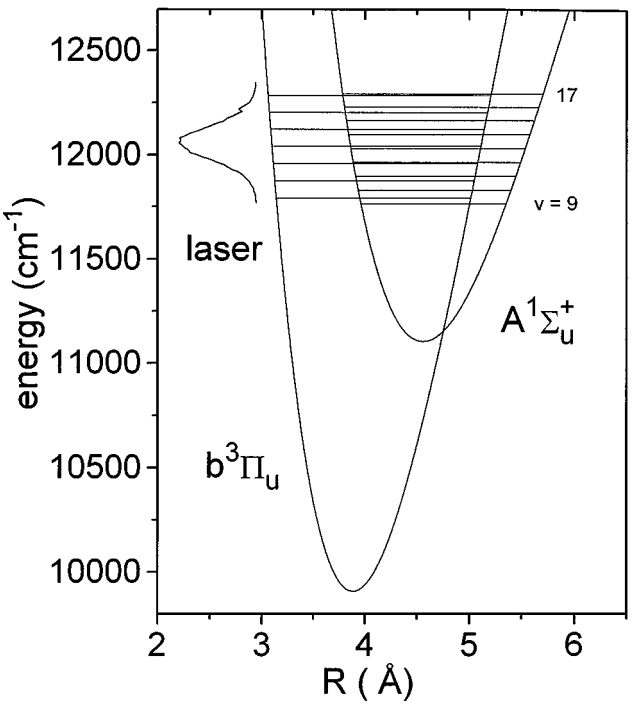


FIG. 2. Perturbation region of the $K_2$ $A\,^1\Sigma_u^+$ state with the $b\,^3\Pi_u$ state. Potential-energy curves and vibrational levels [16] are compared with the spectral position of the excitation laser.

pulse excitation. From the $A$ state the system can evolve to the $b$ state via spin-orbit coupling (SOC). Photoionization out of the $b$ well is negligible, because the resonant intermediate state (2) $^1\Pi_g$ [13] is again a singlet state. A two-photon ionization to a $K_2^+$ triplet state is not probable, because the energy of the ionic triplet states is too high. The ISC process indicates the limits of the Born-Oppenheimer approximation. Two basic approaches can be used to describe these electronic transitions, i.e., the adiabatic and diabatic representations [24]. In the present case the spin-orbit coupling between the $A$ and the $b$ states is rather weak (18.6 $cm^{-1}$) [18] and we can use the diabatic representation. This formalism can be verified ideally in the matrix formalism, which was already used to simulate the pump-probe ionization process in the absence of ISC effects [13]. Basically, the original PES, obtained without spin-orbit coupling, are used as electronic basis functions. The molecular Hamiltonian $H$ is expressed as

$$H(Q,r)=T_{\mathrm{nuc}}(Q)+H_{\mathrm{el}}(r,Q)$$
$$\text{with}\quad H_{\mathrm{el}}(r,Q)=H_{\mathrm{nr}}(r,Q)+H_{\mathrm{so}}(r,Q) \qquad (1)$$

where $T_{\mathrm{nuc}}=P^2/2m$ is the nuclear kinetic energy operator. The electronic Hamiltonian $H_{\mathrm{el}}$ consists of the nonrelativistic electrostatic Hamiltonian $H_{\mathrm{nr}}$ and the spin-orbit-coupling operator $H_{\mathrm{so}}$. The arguments $Q$ and $r$ represent the nuclear and electronic coordinates.

The first-order spin-orbit interaction splits the $b\,^3\Pi_u$ state into its $m_j$ components $\pm2,\pm1,0^{\pm}$ and mainly causes a small energy shift of the coupling $b\,^3\Pi_u$ component with respect to the $A$ state. Therefore, the $b\,^3\Pi_u$ state is prediagonalized, including first-order spin-orbit effects [16] only. According to the selection rules of $H_{\mathrm{so}}$, only the $m_j=0^+$ component of $b\,^3\Pi_u$ couples to the $A$ state by second-order interaction and is included explicitly in the subsequent theoretical quantum-dynamical treatment. The resulting vibronic functions are linear combinations of $A$ and $b$ vibronic functions $\phi_{\mathrm{el},A}\Phi_A$ and $\phi_{\mathrm{el},b}\Phi_b$, where $\phi_{\mathrm{el}}$ are the electronic and $\Phi$ the nuclear eigenfunctions of the $A$ and $b$ state, respectively. The mixing coefficients are given by $(\alpha\langle\phi_{\mathrm{el},A}\Phi_A|H_{\mathrm{so}}|\phi_{\mathrm{el},b}\Phi_b\rangle/\infty|E_{\phi_{\mathrm{el},A}\Phi_A}-E_{\phi_{\mathrm{el},b}\Phi_b}|)$. The influence of the rotational motion [$T_{\mathrm{rot}}\approx18$ ps, rotational revival $T_{\mathrm{rot,rev}}>500$ ps (estimated from [17])] can be neglected in the simulation, because we concentrate our investigations on the short-time dynamics of the ISC process immediately after pump pulse excitation. The time-dependent evolution of the wave packets is evaluated by solving a set of coupled time-dependent Schrödinger equations:

$$i\hbar\frac{\partial}{\partial t}\begin{pmatrix}\Psi_{X\,^1\Sigma_g^+}\\ \Psi_{A\,^1\Sigma_u^+}\\ \Psi_{b\,^3\Pi_{u,0^+}}\\ \Psi_{(2)\,\Pi_g}\\ \Psi_{I,k}(E_k)\end{pmatrix}$$
$$=\begin{pmatrix}H_{XX} & H_{XA} & 0 & 0 & 0\\ H_{AX} & H_{AA} & H_{Ab} & H_{A(2)} & 0\\ 0 & H_{bA} & H_{bb} & 0 & 0\\ 0 & H_{(2)A} & 0 & H_{(2)(2)} & H_{(2)I(E_k)}\\ 0 & 0 & 0 & H_{I(E_k)(2)} & H_{I(E_k)I(E_k)}\end{pmatrix}$$
$$\times\begin{pmatrix}\Psi_{X\,^1\Sigma_g^+}\\ \Psi_{A\,^1\Sigma_u^+}\\ \Psi_{b\,^3\Pi_{u,0^+}}\\ \Psi_{(2)\,^1\Pi_g}\\ \Psi_{I,k}(E_k)\end{pmatrix} \qquad (2)$$

with initial conditions $\Psi_X(Q,t=0)=\Phi_X(Q,v=0)$.

The nuclear wave functions $\Psi_i$ are the projections of the total wave functions on the involved electronic PES. They depend on the nuclear coordinate $Q$ and on the time $t$. $\Phi_X$ is the initial vibrational state $v=0$ of the ground state. The

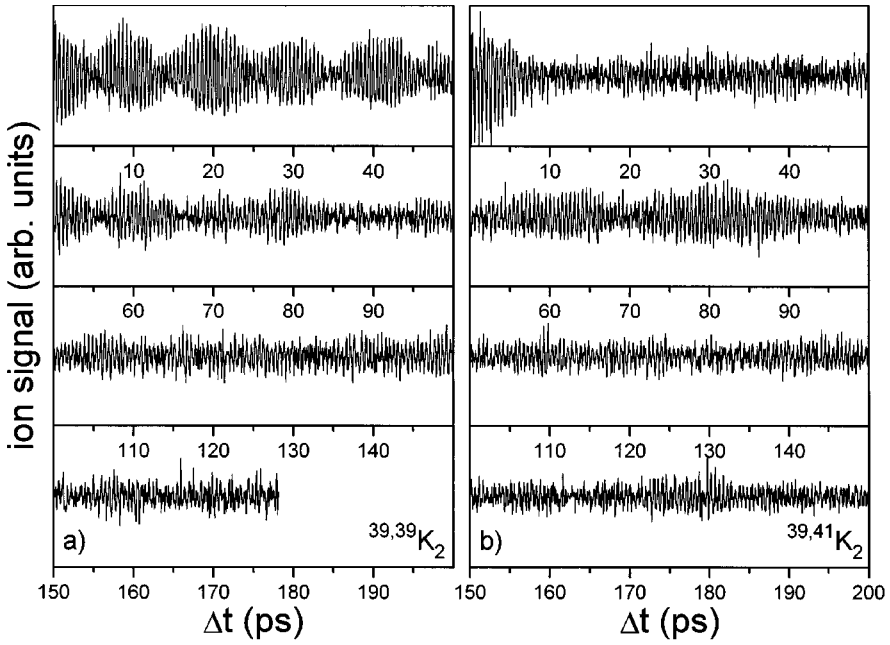


FIG. 3. Temporal evolution of the 3PI signal for the two $K_2$ isotopomers: transient evolution for $^{39,39}K_2$ (a) and $^{39,41}K_2$ (b).

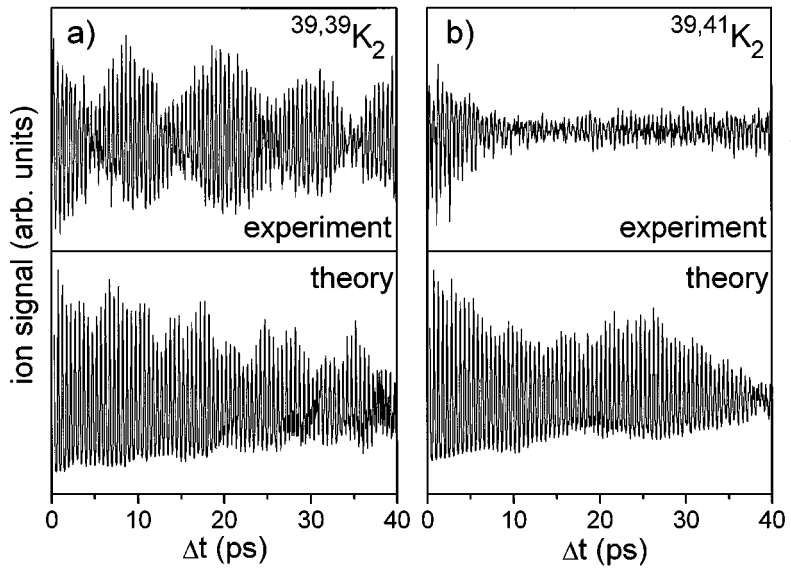


FIG. 4. Comparison of experimental pump-probe spectra and quantum-dynamical pump-probe simulation for $^{39,39}K_2$ (a) and $^{39,41}K_2$ (b). Top panels contain experimental and bottom panels theoretical data.

matrix elements of the Hamiltonian [see Eq. (2)], describing the neutral molecular states, are given by $H_{ii}=T_{\mathrm{nuc}}+V_i$, where $V_i$ represent the potential-energy surfaces $V_i=\langle\phi_{el}|H_{\mathrm{nr}}(Q)+H_{\mathrm{so}}(Q)|\phi_{\mathrm{el}}\rangle_r$.

The time-dependent off-diagonal elements describe the interaction with the laser field in the dipole approximation and are given by $H_{ij}(t)=-\mu_{ij}E(t)$ with the dipole transition moments $\mu_{ij}$. The electromagnetic field $E(t)$ is expressed by $E(t)=E_{\mathrm{pump}}(t)+E_{\mathrm{probe}}(t+\Delta t)$ with $E_{\mathrm{pump/probe}}(t)=E_0\cos(\omega t)s(t)$. $E_0$ is the amplitude of the electromagnetic field, $\omega$ the laser frequency, and $s(t)$ a shape function. Gaussian functions are chosen as adequate shape functions for both pump and probe pulse. For the time-independent off-diagonal elements $\langle b\,^3\Pi_u|H_{\mathrm{so}}|A\,^1\Sigma_u^+\rangle$ a constant value of 18.6 $\mathrm{cm}^{-1}$ is taken from Ref. [18].

Due to the ejection of the electron by the probe laser pulse, a continuum is superimposed on the ion ground state. The interval of the total continuum is [0,0.38 eV]. Different methods of discretizing the electronic continua have been successfully employed in theoretical studies of ultrafast ionization processes [25–27]. Here, the continuum is simulated by discretizing the corresponding energy range by a sufficient number $N$ of electronic states [27]. The matrix elements, representing the continuous part of the Hamiltonian, are given by $H_{Ikk}=\langle\phi_{I,k}|H_I|\phi_{I,k}\rangle$ and $H_{Iki}=\langle\phi_{I,k}|\mu_I(Ek)E(t)|\phi_i\rangle$ with electronic basis functions of the continuum $\phi_{I,k}$ and the electronic wave functions of the neutral state $\phi_i$.

Equation (2) is then solved without further approximation including all multiphoton processes. The solution of Eq. (1) is obtained by the second-order differencing fast-Fourier-transform (SOD-FFT) method [28–30]. The relevant PES for the discussed multiphoton ionization process are the $X$, $A$, $b$, $(2)\,^1\Pi_g$, and the ion states. The PES and the transition dipole moments are obtained from *ab initio* data [14].

## IV. RESULTS AND DISCUSSION

In this section we will first present the results in the time domain obtained by pump-probe experiments, as well as by fully quantum-mechanical simulations. The corresponding results for the frequency domain, calculated by a Fourier analysis will be discussed in Sec. IV B. Finally, we will consider the time-dependent mechanism of the perturbation of the $A\,^1\Sigma_u^+$ state by the $b\,^3\Pi_u$ state.

### A. Time domain

The pump-spectra for $^{39,39}K_2$ and $^{39,41}K_2$ are recorded for delay times between $-5$ ps and more than 180 ps. The temporal evolutions of the ion signal's intensity for both isotopoes are shown in Fig. 3 for delay times between 0 and 200 ps. In both pump-probe spectra a fine oscillatory structure with an oscillation period $T_A\approx 500$ fs—being the full $2\pi$ oscillation time of the wave packet in the $A$ state—is present over the whole range. The first maximum of the oscillation appears at a delay time of 250 fs, being half ($\pi$) of the $A$ state period, such as that of the ionization step that takes place at the outer turning point [13]. This fine oscillation is superimposed on a long-time evolution that reveals totally different features for the two isotopes: the real-time spectrum of $^{39,39}K_2$ [Fig. 3(a)] is dominated by a beat structure with a period $T_{\mathrm{BS}}\approx 10$ ps. A double structure of the beat oscillation maxima appears at $T_{\mathrm{BD},1}\approx 10$ ps and at $T_{\mathrm{BD},2}\approx 60$ ps. For the $^{39,41}K_2$ [Fig. 3(b)] the long-time structure includes different features: A regular dephasing and some fractional revivals [31] are observed. The main revivals appear at 38, 60, and 82 ps.

Quantum-dynamical calculations of the pump-probe spectra for the two isotopes were performed for delay times up to 40 ps. The comparison of the experimental and theoretical ionization signals as a function of the delay time is presented in Fig. 4. In agreement with the experimental data, the short-time dynamics of the theoretical signal show the 500-fs oscillation period of the wave packet prepared in the $A\,^1\Sigma_u^+$ state, and the long-time dynamics reflects the totally different beat structures of the two isotopes. However, the oscillation period of the pronounced and regular beat structure of the isotope $^{39,39}K_2$ [Fig. 4(a)] as well as the faded and irregular beat structure of the isotope $^{39,41}K_2$ [Fig. 4(b)] are somewhat shorter for the theoretical signal. In the case of $^{39,39}K_2$, a period of $T_{\mathrm{BS}}\approx 7.5$ ps, and of about 20 ps in the case of

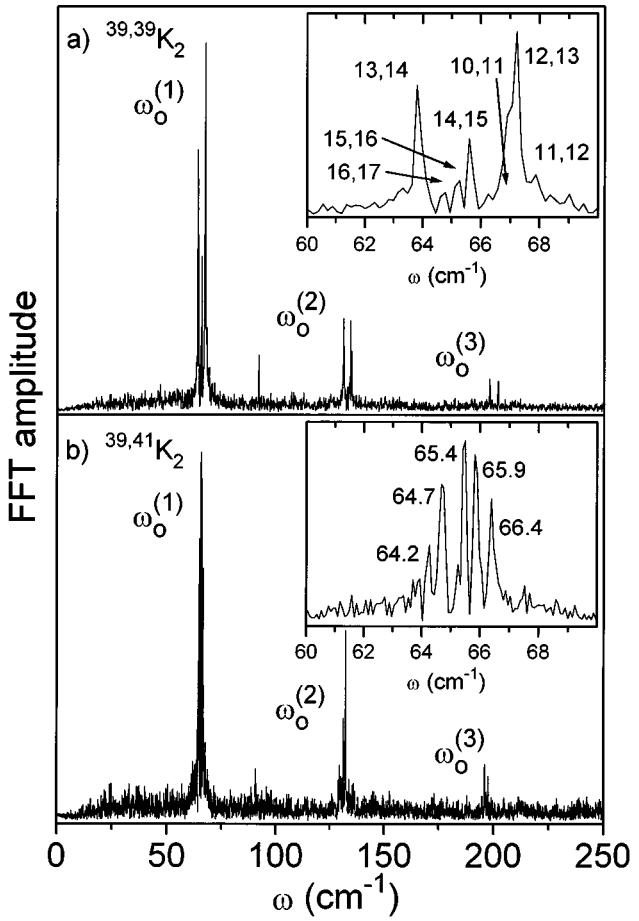


FIG. 5. Calculated Fourier analysis of the normalized pump-probe data for $^{39,39}K_2$ (a) and for $^{39,41}K_2$ (b). The insets describe details of the Fourier spectra between 60 and 70 cm$^{-1}$. The inset of part (a) contains the vibrational level pairs belonging to the frequency components, while in inset (b) the frequency values are given.

$^{39,41}K_2$, is found. The double structure observed in the $^{39,39}K_2$ signal during one beat oscillation period around the delay times $T_{BD,1}$ and $T_{BD,2}$ [Fig. 3(a)] appears even more strongly in the simulation (see Fig. 4).

### B. Frequency domain

The frequency components, involved in the transient spectra, are extracted by a Fourier analysis of the normalized pump-probe data (see Fig. 5). Both Fourier spectra are dominated by a group of frequencies around $\omega_0^{(1)} \approx 65$ cm$^{-1}$. Two additional frequency groups with lower amplitudes appear at $\omega_0^{(2)} \approx 130$ cm$^{-1}$ and at $\omega_0^{(3)} \approx 195$ cm$^{-1}$. An additional peak is observed at $\omega_x \approx 90$ cm$^{-1}$, where the relative intensity is slightly larger in case of the lighter isotopee [Fig. 5(a)].

The frequency group around $\omega_0^{(1)}$ is illustrated in the insets of Fig. 5 for the case of the studied isotopoes. The inset of Fig. 5(a) shows the Fourier components in the pump-probe spectrum of $^{39,39}K_2$. Two main frequencies at 63.8 and 67.2 cm$^{-1}$ dominate this spectrum. The component at 67.2 cm$^{-1}$ seems to be broadened by a component at 66.8 cm$^{-1}$. Further frequency components can be observed at 64.7, 65.2, 65.6, and 67.9 cm$^{-1}$. Hence the wave packet consists of a non-

TABLE I. Vibrational RKR level pairs reached by the excitation laser and respective energy spacings without and with the energy-level shifts for $v=12,13$ of 1.2 cm$^{-1}$ and 2.1 cm$^{-1}$, respectively, in comparison with experimental and theoretical data found for $^{39,39}K_2$.

| $v,v+1$ | $\omega_{RKR}$ (cm$^{-1}$)[a] | $\omega_{shift}$/(cm$^{-1}$)[b] | $\omega_{FFT}$/(cm$^{-1}$)[c] | $\omega_{calc}$/(cm$^{-1}$)[d] |
|---|---|---|---|---|
| 9,10 | 67.35 | [e] | [f] | [f] |
| 10,11 | 67.03 | [e] | 66.8 | [f] |
| 11,12 | 66.71 | 67.91 | 67.9 | [f] |
| 12,13 | 66.40 | 67.30 | 67.2 | 66.8 |
| 13,14 | 66.08 | 63.98 | 63.8 | 62.5 |
| 14,15 | 65.76 | [e] | 65.6 | [f] |
| 15,16 | 65.44 | [e] | 65.2 | [f] |
| 16,17 | 65.11 | [e] | 64.7 | [f] |
| 17,18 | 64.47 | [e] | [f] | [f] |

[a]Vibronic level spacings of Ref. [17].
[b]Level spacings with introduced shifts for $v=12,13$.
[c]Fourier components of pump-probe data.
[d]Main Fourier components of theoretical simulation.
[e]Not changed.
[f]Not observed.

monotonic frequency distribution of the contributing vibrational levels that is manifested as a spectral hole. Instead of the frequency values, corresponding vibrational level pairs are given. These pairs of vibrational levels are found by introducing an energetic shift to the RKR levels of Ref. [17] and by comparing the resulting energy spacings between neighboring levels with the Fourier analysis data (see Table I). Introducing a shift for $v=12$ and $v=13$ of 1.2 and 2.1 cm$^{-1}$, respectively, results in a good agreement. The two dominant frequencies, observed in the pump-probe spectrum, can clearly be proved to be responsible for the beat oscillation period of $T_{BS} \approx 10$ ps. Overlaying the frequencies $\omega_{13,14}=63.8$ cm$^{-1}$ and $\omega_{12,13}=67.2$ cm$^{-1}$ leads to a period of $T_{BS}=9.8$ ps. For the isotopoe $^{39,41}K_2$ the spectrum around 65 cm$^{-1}$ is presented in the inset of Fig. 5(b). We observe five distinct components in the frequency group at 64.3, 64.7, 65.5, 65.9, and 66.4 cm$^{-1}$. Here, the numbering is not included due to missing spectroscopic data for this isotopoe.

The Fourier spectra were calculated as well for the theoretical data. Since the simulations were performed up to 40 ps, only, the two main frequencies $\omega_{calc1,2}$ are solely resolved (see Table I). The resulting frequencies $\omega_{calc1}=66.8$ and $\omega_{calc\ 2}=62.5$ cm$^{-1}$ lead to the period $T_{BS}=7.8$ ps. The difference between experimental and theoretical findings in the ion signal originates from the deviation of the *ab initio* PES from the observable potential (compare with [17,18]).

Experimental and theoretical Fourier spectra reveal the effect of the spin-orbit coupling to the $b\,^3\Pi_u$ state. In the region of the pump laser pulse the perturbation is most effective in the isotope $^{39,39}K_2$. Two vibrational levels of the $b\,^3\Pi_u$ state ($v=23,24$) are close [16,18], nearly energetically degenerated, to the two vibrational levels of the $A\,^1\Sigma_u^+$ state ($v=12,13$), and induce the shift of these perturbed vibronic $A$ state levels [as seen in the inset of Fig. 5(a)]. For $^{39,41}K_2$ the situation is different. In the excitation range of the pump pulse no effective perturbation is found. All vibrational levels contributing to in the wave packet are perturbed, but only

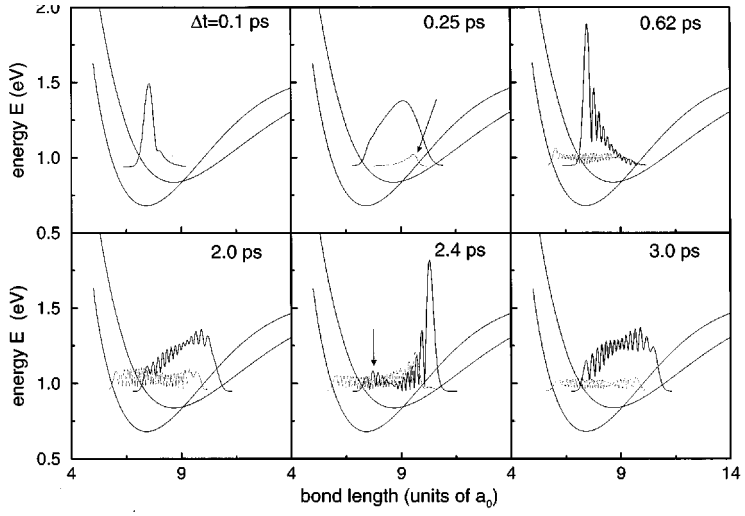


FIG. 6. Snapshots of the ISC process induced by spin-orbit coupling between the $A\,^1\Sigma_u^+$ state and the $b\,^3\Pi_u$ state during and after pump pulse excitation for selected delay times.

to a small amount [see Fig. 5(b)]. The regular pattern of an unperturbed spectrum (see, e.g., [2]) is conserved.

### C. Mechanism

In this final subsection we will follow the buildup and the time dependence of the induced electronic population dynamics. Subsequently, we will analyze whether, in addition to the vibrational dynamics, the electronic population dynamics is detectable time resolved in the ion signal.

The temporal evolution of the radiationless transition is illustrated by a sequence of representative wave packets $\Psi_{A\,^1\Sigma_u^+}(Q,t)$ and $\Psi_{b\,^3\Pi_u}(Q,t)$ resulting from the solution of the coupled Schrödinger equation [Eq. (2)] in the time domain 0.1 ps$\leqslant t \leqslant$3.0 ps (Fig. 6). From $\Psi_{A\,^1\Sigma_u^+}(Q,t)$ and $\Psi_{b\,^3\Pi_u}(Q,t)$, the total population $P$ of the electronic states $A\,^1\Sigma_u^+$ and $b\,^3\Pi_u$ is derived:

$$P(A\,^1\Sigma_u^+,t) \equiv \int_{Q_l}^{Q_u} |\Psi_{A\,^1\Sigma_u^+}(Q,t)\Psi_{A\,^1\Sigma_u^+}(Q,t+\Delta t)|\,dQ \tag{3a}$$

and

$$P(b\,^3\Pi_u,t) \equiv \int_{Q_l}^{Q_u} |\Psi_{b\,^3\Pi_u}(Q,t)\Psi_{b\,^3\Pi_u}(Q,t+\Delta t)|\,dQ, \tag{3b}$$

with $Q_l = 5.0a_0$ and $Q_u = 15.0a_0$ the lower and upper limits of the spatial grid. The total populations of both states are presented for two different time periods, up to 3 ps in Fig. 7 and up to 20 (80 ps) in Fig. 8.

First we discuss the ISC process for the more effective perturbation in the isotope $^{39,39}K_2$. The results, presented in Figs. 6 and 7, point to the details of how the ISC process is built up. Figure 6 shows selected snapshots of representative wave packets during the first oscillation period of the electronic populations $P(A\,^1\Sigma_u^+,t)$ and $P(b\,^3\Pi_u,t)$ (Fig. 7).

The wave packet is created by the pump laser at the inner turning point of the $A$ state (first snapshot in Fig. 6). Energetically, the wave packet is located about 0.1 eV above the electronic curve crossing. The ISC occurs for the first time at about 250 fs (second snapshot in Figs. 6 and 7), when the center of the wave packet $\Psi_{A\,^1\Sigma_u^+}(Q,t)$ approaches the outer turning point of the $b$ state (at $Q = 9.5a_0$). It is to be noted that the transition $A\,^1\Sigma_u^+ \rightarrow b\,^3\Pi_u$ takes place at the outer turning point of the $b$ state and not at the location of the curve crossing at $Q = 8.9a_0$, contrary to other findings [23].

As soon as some fraction of $\Psi_{^3\Pi_u}(Q,t)$ has been created, the wave packet begins to propagate according to its own time-dependent phase relation (see Fig. 6). When the wave

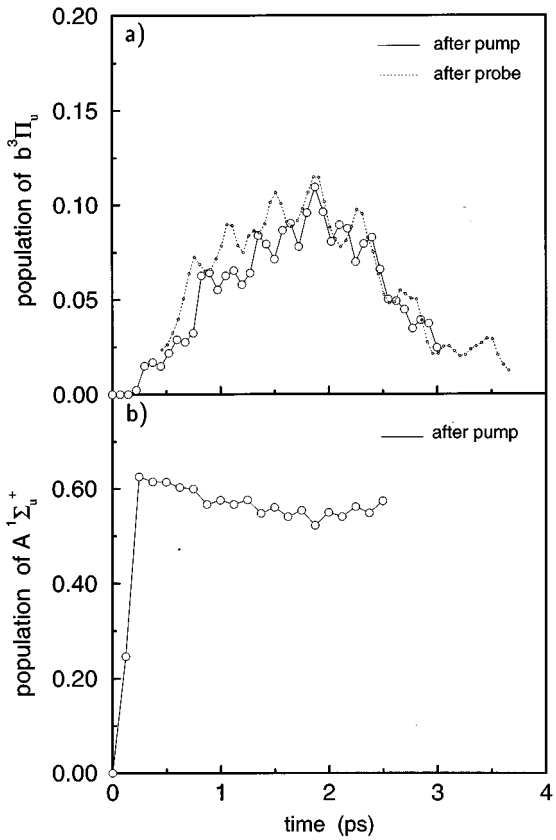


FIG. 7. Electronic population in $A\,^1\Sigma_u^+$ and $b\,^3\Pi_u$ states during and after pump pulse excitation for a time period of 3 ps. In panel (a) the population of the $b\,^3\Pi_u$ state after pump (—) and after probe (···) pulse excitation is presented. The probe pulse intensity is reduced by a factor of 10. In panel (b) the population in the $A$ state after excitation with the pump pulse is shown.

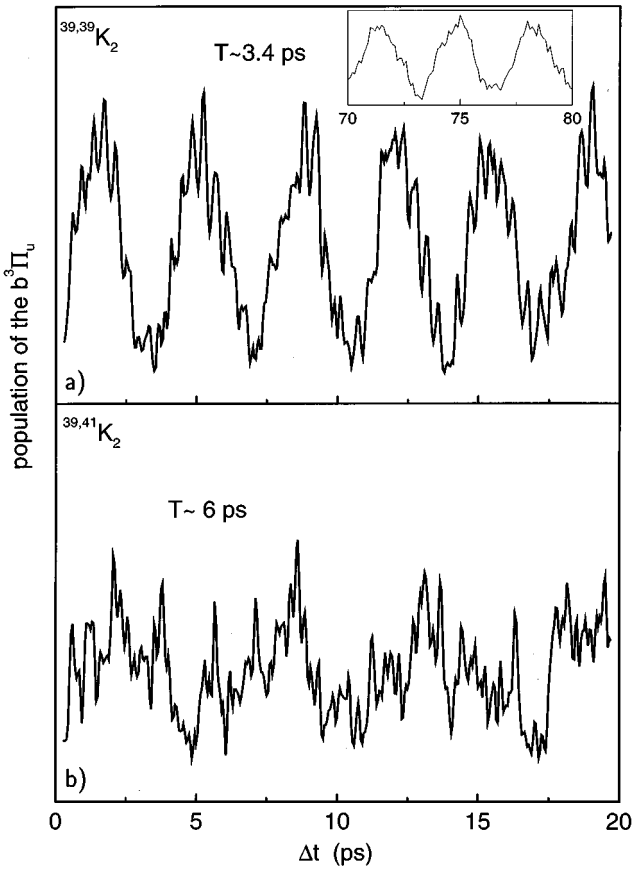


FIG. 8. Electronic population in the $A\,^1\Sigma_u^+$ and $b\,^3\Pi_u$ states during and after pump pulse excitation for the isotopomers $^{39,39}K_2$ (a) and $^{39,41}K_2$ (b) for a propagation time of 20 ps.

packet $\Psi_{b\,^3\Pi_u}(Q,t)$ passes the inner turning point of the $A$ state ($Q=8.22a_0$), some fraction of $\Psi_{b\,^3\Pi_u}(Q,t)$ is transferred back into the $A$ state (see Fig. 6 for the delay times 0.62 and 2.4 ps). These back and forth transitions give rise to the fine oscillations superimposed on the low-frequency beating in the population probabilities $P(A\,^1\Sigma_u^+,t)$ and $P(b\,^3\Pi_u,t)$ (Figs. 7 and 8). The oscillation period of 224 fs corresponds to the vibrations of a wave packet in the corresponding ''adiabatic'' potential, characterized by the inner turning point of the $A$ state and the outer turning point of the $b$ state. Evidently, the vibrational energy transfer in a bound-state system from one electronic state into another occurs most probably at the turning point of the actual receiver state. Possible reasons are, of course, favorable Frank-Condon (FC) factors of the involved wave packets and the near zero kinetic energy of the newly prepared portion of the wave packet.

Similar findings for coupled bound-state systems were reported for several model studies by Stock and Domcke [20,21]. For dissipative systems, Zewail and co-workers [32,33] observed a step function superimposed on an exponential increase, revealing in this case one optimal location for the non-Born-Oppenheimer transition in one direction only. In $^{39,39}K_2$ the low-frequency oscillation period of the electronic population is proportional to the effective perturbation matrix element (see Sec. III) between them. The first maximum of the $b$ state population is reached at 1.87 ps (Fig. 7), which means that the $A\,^1\Sigma_u^+ \rightarrow b\,^3\Pi_u$ ISC occurs within a time scale of $\tau_{ISC}\approx 2$ ps. The relative changes of the amplitude of $P(A\,^1\Sigma_u^+ t)$ are rather small (about 8%). The dotted curve in Fig. 7(a) presents the population in the $b$ state after probe pulse interaction. Fine oscillations are still recognizable, but evidently the probe laser pulse slightly averages over the fast oscillations.

The period of the low-frequency beating period is 3.754 ps (Fig. 8), which corresponds to the average energy splitting (about 8 $cm^{-1}$) of the two closely spaced pairs of $A$ and $b$ vibronic levels. This oscillatory structure remains constant [see small inset in Fig. 8(a)] and is reflected in the double peak structure superimposed on the 10-ps beat structure in the ion signal [Figs. 3(a) and 4]. As pointed out already in Sec. IV A, the beating period $T_{BS}\approx 10$ ps originates from the shifted vibronic levels in the $A\,^1\Sigma_u^+$ state. For delay times larger than 80 ps, when the beat structure vanishes in the ion signal, the fast oscillations on the $b\,^3\Pi_u$ population also begin to disappear. Both observations are due to the known spreading of the wave packet in the $A$ state [13].

For the less perturbed isotope $^{39,41}K_2$, the perturbation is more delocalized over several vibrational levels. The amount of population and energy transfer is smaller and slower (Fig. 8). The resulting time scale of ISC induced by SOC is $\tau_{ISC}\approx 6$ ps and the electronic population oscillates with a longer period of 7 ps. Moreover, the low-frequency beating loses its pronounced characteristics (Fig. 8) and consequently no structure is superimposed on the ion signal.

## V. SUMMARY

We demonstrated experimentally and theoretically, that the femtosecond pump-probe technique can be used as a highly sensitive method to study excited vibrational states and their perturbation due to crossing electronic states. For our investigations we chose the two isotopes $^{39,39}K_2$ and $^{39,41}K_2$, and excited them with ultrashort laser pulses of 833 nm in their $A$ state. Two neighboring levels of $^{39,39}K_2$ are strongly perturbed by the excited electronic $b$ state while nearly no perturbation for the other isotopoe is observed. It should be pointed out that under different excitation conditions a similar perturbation might occur in the heavier isotopomer. No perturbation at all was found at 840 nm [13].

The high stability of our employed molecular beam, as well as the high repetition laser pulse source, enabled the scanning of the time evolution of the wave packet prepared on the $A$-state PES even for the rather rare isotopoe $^{39,41}K_2$ over 200 ps with high time resolution and an excellent signal-to-noise ratio. Fourier spectra of better than 0.1 $cm^{-1}$ spectral resolution for both the perturbed and unperturbed system were obtained. While the perturbed system presents a fascinating beat structure of high regularity in the time domain, the unperturbed system shows up the more regular Fourier spectra, but besides the fast 500-s oscillation a rather low temporal structure. By comparison of theoretical simulations and experimental results, the characteristics of the observed vibrational states are neatly observable and well understood for both isotopes. It is to be noted that the beat structure in $^{39,39}K_2$ is due to the spectral hole in the frequency distribution of the $A$-state wave packet. It is, how-

ever, not related to interferences of wave packets propagating on different electronic PES as reported for $Na_2$ at 620 nm [4]. From the theoretical treatment we were able to observe the buildup of an ISC process that strongly influences the temporal evolution of the PI signal in the perturbed case. This analysis revealed that under the given experimental conditions it was possible to detect the low-frequency mode of the electronic population dynamics superimposed as a double peak structure on vibrational dynamics in the 3PI signal.

**ACKNOWLEDGMENTS**

The authors are indebted to Professor Ludger Wöste. The experiment was performed at his laboratories. His great enthusiasm and extraordinary wealth of ideas were an important basis for the performed experiment. The authors would also like to thank Professor J. Manz for many stimulating discussions. Generous financial support by the Deutsche Forschungsgemeinschaft DFG through Project No. SFB 337 and a Habilitationsstipendium (for R. dV.-R.) is gratefully acknowledged.

[1] M. Dantus, R. M. Bowman, and A. H. Zewail, Nature **343**, 737 (1990).
[2] M. Gruebele, G. Roberts, M. Dantus, R. M. Bowman, and A. H. Zewail, Chem. Phys. Lett. **166**, 459 (1990).
[3] M. Gruebele and A. H. Zewail, J. Chem. Phys. **98**, 883 (1993).
[4] T. Baumert, M. Grosser, R. Thalweiser, and G. Gerber, Phys. Rev. Lett. **67**, 3753 (1991).
[5] I. Fischer, D. M. Villeneuve, M. J. J. Vrakking, and A. Stolow, J. Chem. Phys. **102**, 5566 (1995).
[6] M. J. J. Vrakking, I. Fischer, D. M. Villeneuve, and A. Stolow, J. Chem. Phys. **103**, 4538 (1995).
[7] T. Baumert, V. Engel, C. Meyer, and G. Gerber, Chem. Phys. Lett. **200**, 488 (1992).
[8] Ch. Meier and V. Engel, Chem. Phys. Lett. **212**, 691 (1993).
[9] J. M. Papanikolas, R. M. Williams, P. Kleiber, J. L. Hart, C. Brink, S. D. Price, and S. R. Leone, J. Chem. Phys. **103**, 7269 (1995).
[10] V. Engel, Chem. Phys. Lett. **178**, 130 (1990).
[11] T. Baumert, V. Engel, C. Röttgermann, W. T. Strunz, and G. Gerber, Chem. Phys. Lett. **191**, 639 (1992).
[12] Ch. Meier and V. Engel, J. Chem. Phys. **101**, 2673 (1994).
[13] R. de Vivie-Riedle, B. Reischl, S. Rutz, and E. Schreiber, J. Phys. Chem. **99**, 16829 (1995).
[14] R. de Vivie-Riedle, K. Kobe, J. Manz, W. Meyer, B. Reischl, S. Rutz, E. Schreiber, and L. Wöste, J. Phys. Chem. (to be published).
[15] V. Blanchet, M. A. Bouchene, O. Cabrol, and B. Girard, Chem. Phys. Lett. **233**, 491 (1995).
[16] A. J. Ross, P. Crozet, C. Effantin, J. d'Incan, and R. F. Barrow, J. Phys. B **20**, 6225 (1987).
[17] A. M. Lyyra, W. T. Luh, L. Li, H. Wang, and W. C. Stwalley, J. Chem. Phys. **92**, 43 (1990).
[18] G. Jong, L. Li, T.-J. Whang, and W. C. Stwalley, J. Molec. Spectrosc. **155**, 115 (1992).
[19] A. J. Ross, Ph.D. thesis, Université Claude Bernard–Lyon I, Lyon, 1987 (unpublished).
[20] G. Stock and W. Domcke, Chem. Phys. **124**, 227 (1988).
[21] G. Stock and W. Domcke, J. Phys. Chem. **97**, 12 466 (1993).
[22] L. Seidner and W. Domcke, Chem. Phys. **186**, 27 (1994).
[23] C. Daniel, M.-C. Heitz, J. Manz, and C. Ribbing, Chem. Phys. **102**, 905 (1995).
[24] R. Schinke, *Photodissociation Dynamics*, Cambridge Monographs on Atomic, Molecular and Chemical Physics (University Press, Cambridge, England, 1993).
[25] R. S. Burkey and C. D. Cantrell, J. Opt. Soc. Am. B **1**, 169 (1984).
[26] R. S. Burkey and C. D. Cantrell, J. Opt. Soc. Am. B **2**, 451 (1985).
[27] B. W. Shore, Chem. Phys. Lett. **99**, 240 (1983).
[28] R. Kosloff and D. Kosloff, J. Chem. Phys. **79**, 1823 (1983).
[29] D. Kosloff and R. Kosloff, J. Comput. Phys. **52**, 35 (1983).
[30] R. Kosloff, J. Phys. Chem. **92**, 2087 (1988).
[31] I. Sh. Averbukh and N. F. Perelmann, Phys. Lett. A **139**, 449 (1989).
[32] M. Rosker, T. S. Rose, and A. H. Zewail, Chem. Phys. Lett. **146**, 175 (1988).
[33] T. S. Rose, M. Rosker, and A. H. Zewail, J. Chem. Phys. **88**, 6672 (1988).